Conductance Switching in an Asymmetric Single-molecule Junction

Masato Takei,[a,b] Akira Takatsuki,[a,b] Katsunori Wakabayashi,[c] Satoshi Kaneko,[d] Hiroshi Suga,*[a,b] Yasuhisa Naitoh**,[e] and Kazuhito Tsukagoshi***,[b,a]

[a] Chiba Institute of Technology, Tsudanuma, Narashino, Chiba 275-0016, Japan

[b] International Center for Materials Nanoarchitectonics (WPI-MANA), National Institute for Materials Science (NIMS), Tsukuba, Ibaraki 305-0044, Japan

[c] Department of Nanotechnology for Sustainable Energy, School of Science and Technology, Kwansei Gakuin University, Sanda, Hyogo 669-1330, Japan

[d] Department of Materials Science and Engineering, School of Materials and Chemical Technology, Institute of Science Tokyo, Tokyo 152-8550, Japan

[e] Core Electronics Research Institute, National Institute of Advanced Industrial Science and Technology (AIST), Tsukuba, Ibaraki 305-8565, Japan

Keywords: fullerene, C_{60} pyrrolidine tris-acid, single-molecule device, metal migration, single-level transport model, transition voltage spectroscopy

ABSTRACT

Electric switching in a single-molecule junction based on the asymmetric C_{60} pyrrolidine tris-acid (CPTA) molecule was demonstrated using nanogap electrodes spin-coated with a CPTA thin film. Among the embedded molecules, those closest to the cathode were preferentially activated during two-terminal conductance measurements, exhibiting reproducible bistable switching between low- and high-conductance states at room temperature. The CPTA molecule was anchored to the cathode via a carboxyl ligand, while the opposing electrode was positioned to allow modulation of the molecule–electrode distance by an applied bias voltage. This configuration enabled two distinct transport regimes: metal–fullerene conduction in the high-conductance state and through-space tunneling across a metal–CPTA–vacuum–metal junction in the low-conductance state. Analysis of the high-conductance state using the single-level tunneling transport model confirmed that charge transport occurred through a single molecule, despite the film-based fabrication. In the low-conductance state, transition voltage spectroscopy revealed that the junction asymmetry parameter was strongly dependent on the through-space distance between the fullerene cage and the opposing electrode, offering insight into structural modulation during switching.

■ INTRODUCTION

The continuous drive for miniaturization in electronic devices has spurred extensive research into molecular-scale components.[1–15] Among various miniaturization strategies, single-molecule junctions represent the ultimate limit in size for switching elements.[2,16–22] However, constructing such junctions remains technically demanding, primarily due to the challenges in fabricating nanometer-scale electrode gaps and positioning individual molecules within these gaps with atomic precision. Traditional studies on single-molecule junctions have typically required the fabrication of numerous devices, followed by individual electrical characterization to identify suitable candidates for detailed investigation.

Mechanically controllable break junction (MCBJ) and scanning tunneling microscopy break junction (STMBJ) techniques are widely employed to fabricate single-molecule junctions.[19,21,23–26] A key advantage of these methods is their tunable electrode gap, which facilitates molecular connection. However, both approaches face significant technical challenges in integrating large numbers of single-molecule junctions as functional electrical switching elements. The MCBJ method, which utilizes piezoelectric actuators or substrate bending, requires bulky equipment and is ill suited for parallel operation of multiple devices. Similarly, STMBJ relies on atomic-scale probe manipulation, making it impractical for large-scale fabrication. Despite these limitations, both techniques have contributed significantly to the fundamental demonstration of molecular electronic devices.[23,27–29]

Efficient incorporation of molecules into metallic junctions within solid-state devices is critical for future molecular electronics applications.[1,30] Conventional static nanogap electrodes fabricated on Si substrates suffer from fixed electrode spacing, leading to low molecular insertion efficiency and hindering further development. While the integration of billions of molecular switches still remains a challenge, we have developed an alternative strategy based on molecular self-assembly combined with nanogap tunability to enable reliable switching operation.

In this study, C_{60} pyrrolidine tris-acid (CPTA) molecules were incorporated into nanogap electrodes via spin-coating of a CPTA solution. The carboxyl ligands of CPTA served to anchor the molecule to the cathode. The electrical connection between the C_{60} cage and the opposing electrode was modulated through applied bias voltage. Cyclic voltage sweeps induced repeatable, bistable conductance switching between high-conductance state (HCS) and low-conductance state (LCS). The assembled molecular device exhibited stable

switching over more than 100 cycles, with an on/off ratio exceeding 100. The HCS, corresponding to a metal–CPTA–metal junction, was analyzed using the single-level tunneling transport (SLTT) model. This revealed that electron tunneling was governed by an energy offset (ε_0) of 0.82 eV between the metal Fermi level and the molecular conduction orbital. The LCS, attributed to through-space tunneling across a metal–CPTA–vacuum–metal junction, was evaluated using transition voltage spectroscopy (TVS).[31–36] The ratio of the transition voltage (V_{trans}) to ε_0 in the Fowler–Nordheim (FN) plot reflected the junction's overall asymmetry, allowing electrical monitoring of structural changes.[37] Variations in the asymmetry parameter (η) indicated an increased transport distance between the molecule and the anode in the LCS, consistent with metal atom migration at the anode. Moreover, the continuous modulation of η demonstrated the device's capability for multistate conductance switching.

■ EXPERIMENTAL

The molecular switch was fabricated by combining electron-beam lithography, controlled electrical metal migration, and spin-coating of a CPTA molecular solution (Figure 1a). To ensure uniform coating of the CPTA film, a 2-nm-thick AlO_x layer was deposited on a Si substrate with a 250-nm thermal oxide layer via atomic layer deposition. Subsequently, a 200-nm-wide metal wire was patterned using electron-beam lithography. A 10-nm-thick AuPd (8:2) alloy was then deposited to form the metal wire on the substrate.

Electromigration was employed to create nanoscale electrodes separated by a nanogap, enabling through-space electron tunneling. A continuous metal wire was intentionally broken by applying a high-density current under feedback-regulated voltage control.[38–40] The initial application of bias voltage under vacuum allowed electron transport through the nanogap, with the tunneling current dependent on both the gap length and the electrode surface work function. Fitting the resulting current–voltage (I–V) characteristics using the Simmons model estimated the gap length to be approximately 0.7 nm or slightly larger.[41] It is well established that as a result of electromigration, the anode side of the nanogap tends to undergo more pronounced atomic migration, while the cathode side remains relatively stable.[42–45]

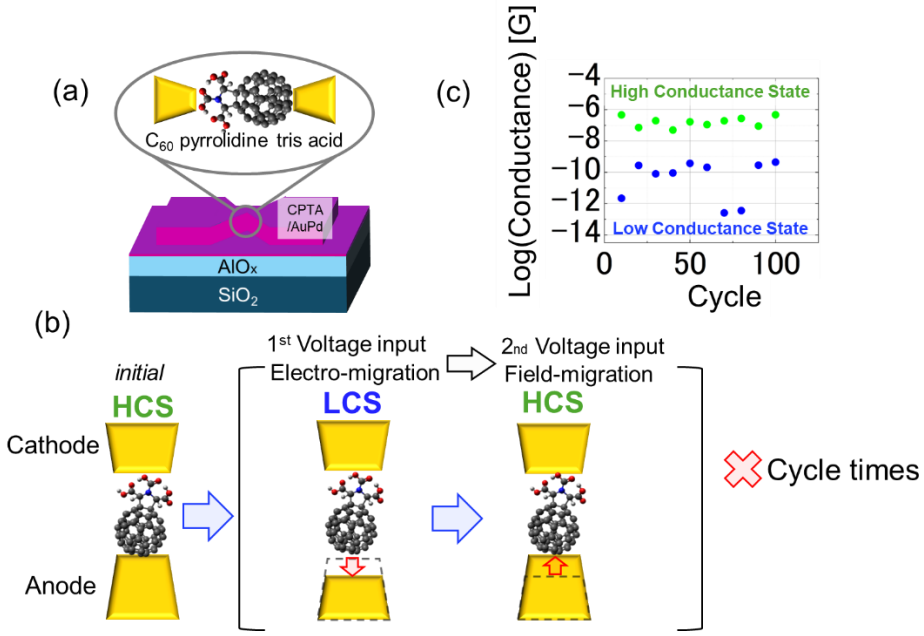

97

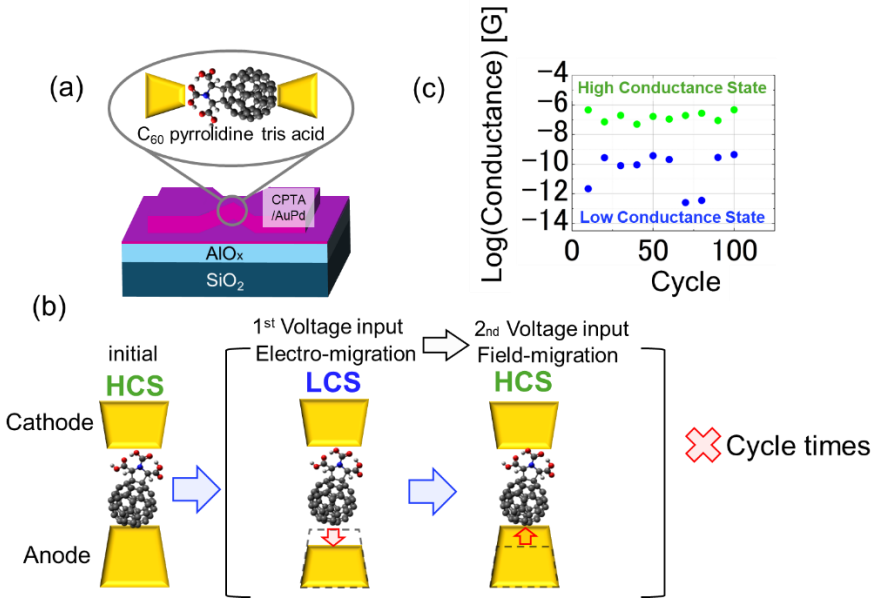

98

99 **Figure 1.** (a) Schematic of the CPTA junction. (b) Single-molecule switch model based on
100 electromigration and field migration. (c) Observed conductance switching between two
101 states: high-conductance state (HCS) and low-conductance state (LCS). Each point
102 represents an average over 10 cycles.

103

A CPTA film approximately 2 nm thick was spin-coated from a dimethylformamide solution, uniformly covering both the electrodes and the insulating surface (Figure 1a). CPTA was chosen as the switching element due to its structural asymmetry and site-selective bonding characteristics. The carboxyl ligands of CPTA can form stable bonds with oxygen-deficient surface sites (Figure 1b).[46] This stability is likely facilitated by oxidation of surface Pd atoms, enabling robust anchoring of CPTA molecules. Among the CPTA molecules present within the nanogap, the one closest to the electrodes typically dominates electrical conduction when a bias voltage is applied. Upon initial conduction, the current increases nonlinearly and reaches a relatively high level. Subsequently, due to electromigration, the anode surface tends to retract from the CPTA molecule—especially when the molecule is anchored to the cathode.[4,43] This displacement creates a through-space gap, thereby suppressing the tunneling current.

Once the through-space gap forms, applying a bias voltage from zero can induce surface ionization under a strong electric field, triggering a process known as field migration.[4,43] This drives the metal edge to shift back toward the CPTA molecule (Supporting Information S1), re-establishing conduction through the molecular junction. The through-space separation in the junction can thus be externally modulated by the applied bias voltage, enabling cyclic switching behavior (Figure 1c, Supporting Information S2). Such reversible shifts of the anode surface—governed by the interplay of electromigration and field migration—are also observed in scanning tunneling microscope systems.[43]

The LCS, characterized by an open through-space gap, is defined as the OFF state, while the HCS, where the gap is closed, corresponds to the ON state (Figure 1c). Transitioning from the OFF (LCS) to the ON (HCS) state is achieved by applying a small bias voltage, which induces a nonlinear increase in current and promotes field migration, thereby closing the through-space. When a higher voltage is applied, an overcurrent can occur, resulting in the appearance of negative differential resistance (NDR) in the *I–V* curve. This overcurrent triggers the reopening of the through-space, switching the junction back to the OFF state (LCS).

Conversely, when the CPTA molecule is anchored to the anode surface, the initial current induces electromigration, potentially causing the anode metal to retract and create a through-space gap. Once this gap forms, the CPTA molecule—now positioned on the anode side—no longer contributes effectively to tunneling conduction due to its unfavorable spatial configuration, despite lowering the local work function compared to the bare metal surface.[47–49] As a result, the overall current through the junction is significantly reduced.

In this model, only approximately half of the CPTA molecular junctions are statistically expected to participate in cyclic switching, due to the asymmetry in electrode anchoring. However, in practical devices, conduction can be taken over by the CPTA molecule positioned at the second-shortest electrode distance if the primary molecule (at the first-shortest electrode distance) is deactivated on the anode side. If this second molecule is also anchored to the anode, it too becomes inactive, allowing a cathode-anchored molecule to potentially assume the switching role.

To support this proposed switching mechanism, two key factors must be considered: (1) the involvement of single-molecule transport, and (2) the activation and switching functionality of asymmetrically anchored CPTA molecules on the cathode electrode.

To confirm single-molecule transport, the metal–CPTA–metal junction was characterized in the HCS. Under HCS conditions, the nanogap length was systematically varied (Supporting Information S1), and junction conductance was recorded to construct a conductance histogram (Figure 2). The occurrence frequency (φ) of the metal–CPTA–metal junction and that of a reference nanogap junction without CPTA were plotted as a function of junction conductance over 2000 switching cycles. Both junction types exhibited a peak in occurrence frequency; however, their most probable conductance values differed significantly. The reference junction without CPTA showed higher conductance, indicating that the presence of CPTA increases the overall junction resistance (Figure 2). The differential conductance characteristics between the CPTA and reference junctions were extracted (inset, Figure 2), confirming that the insertion of the resistive CPTA molecule reduces overall conductance—supporting the conclusion that single-molecule transport is responsible for the observed behavior.

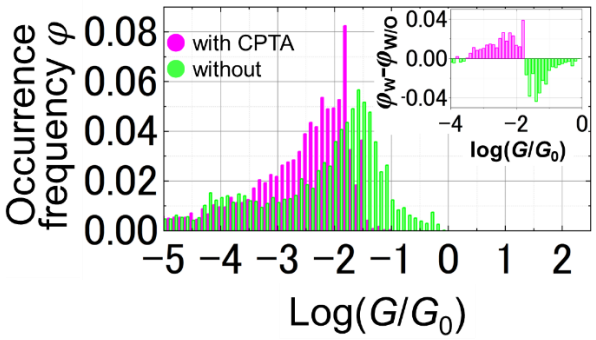

Figure 2. Conductance histogram obtained in the junction with and without CPTA. Detailed procedures are mentioned in Supporting Information S1. The vertical axis (φ) represents the occurrence frequency. Inset: Difference histogram of occurrence of the junctions with and without CPTA. The occurrence frequency of the CPTA junction exhibited a peak at −2.3 G/G_0.

A standard analytical approach based on the SLTT model was employed to evaluate the molecular junction, assuming electron transport occurs via a specific molecular energy level.[29,42] The SLTT model describes the current ~~$I(V)$~~ through the junction as

$$I(V) = \frac{8e}{h}\frac{\Gamma_1\Gamma_2}{\Gamma_1+\Gamma_2}\left\{\tan^{-1}\left(\frac{\frac{\Gamma_2}{\Gamma_1+\Gamma_2}eV-\varepsilon_0}{\Gamma_1+\Gamma_2}\right)+\tan^{-1}\left(\frac{\frac{\Gamma_1}{\Gamma_1+\Gamma_2}eV+\varepsilon_0}{\Gamma_1+\Gamma_2}\right)\right\}, \quad (1)$$

where ε_0 is the energy offset between the Fermi level of the electrodes and the molecular conducting orbital, and Γ_1 and Γ_2 are the coupling strengths of the molecule to the left and right electrodes, respectively (Figure 3a). The value of ε_0 was estimated from conductance measurements obtained under varying nanogap conditions across 2000 switching cycles (Supporting Information S1). The total coupling strength $\Gamma = \Gamma_1 + \Gamma_2$ was extracted from the corresponding current values in each cycle. The extracted values of ε_0 and Γ are plotted in Figure 3b, showing consistent and reproducible overlap across all measurements. Statistical analysis yielded average values of ε_0 and Γ are 0.82 ± 0.024 eV and 0.08 ± 0.004. Notably, the extracted ε_0 is comparable to that reported for single C_{60} molecular junctions ($\varepsilon_0 \approx 0.60$ eV), further supporting the conclusion that charge transport occurs through a single CPTA molecule.[29]

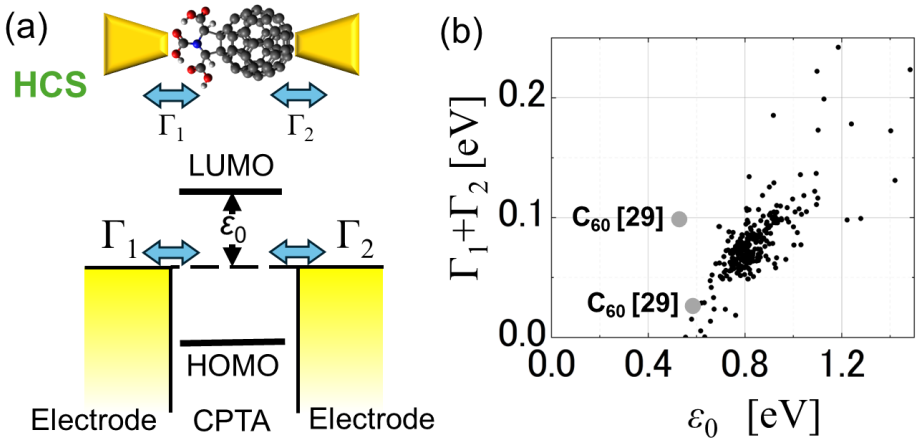

Figure 3. (a) Schematic of the resonant tunneling model mediated by molecular orbitals. In the SLTT model, the tunneling process is described using the coupling Γ and ε_0 between the conducting orbital and Fermi level. (b) ε_0 and Γ values extracted using the SLTT model from *I–V* characteristics obtained in the range of −1 to +1 V in the HCS.

Previous studies using MCBJ have reported $\varepsilon_0 \approx 0.60$ eV for single C_{60} molecular junctions.[29] The conducting orbital (lowest unoccupied molecular orbital) of CPTA is known to lie approximately 0.2 eV higher than that of C_{60}.[46,50] Additionally, the Fermi level of the AuPd (8:2) alloy used in this study may be slightly higher than that of pure Au, potentially leading to an underestimation of ε_0 by up to 0.1 eV.[51] Taking into account these factors and the measurement fluctuations, the observed ε_0 value is consistent with charge transport through a single CPTA molecule.

In the LCS, the junction adopts a metal–CPTA–vacuum–metal configuration, which is inherently structurally asymmetric. The experimental observations in this state were analyzed using the TVS model.[31–37] TVS correlates the transition voltage (V_{trans})—identified by a change in the slope of the FN plot—with the energy offset and the asymmetry parameter (η) of the junction, providing insights into structural variations. Replotting the experimental *I–V* characteristics across junctions with varying conductance in FN coordinates revealed that FN tunneling features were absent at a conductance of 3 mG_0, and V_{trans} systematically shifted to lower values as conductance decreased. This trend indicates an increasing through-space gap

in lower-conductance junctions (dashed line, Figure 4a), consistent with a structurally evolving junction geometry in the LCS.

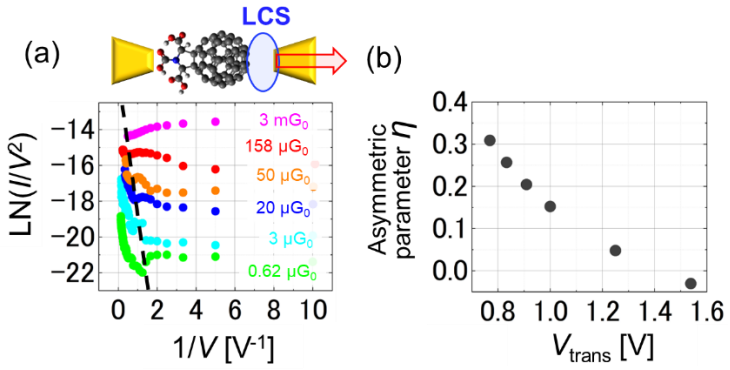

Figure 4. (a) TVS analysis of the CPTA device. The dashed lines in the figure guide readers to see the transition voltage of FN tunneling. (b) Extracted asymmetry parameter using V_{trans} obtained in (a).

To evaluate the structural dependence of charge transport in the molecular junction, η was extracted using TVS analysis (Figure 4b).[36] The asymmetry parameter is defined as

$$\eta = \frac{\varepsilon - 0.85 \times V_{trans}}{2.3 \times V_{trans}}, \quad (2)$$

where η ranges between −0.5 and 0.5. In a fully asymmetric junction, η approaches ±0.5. A positive η indicates a larger voltage drop on the anode side, while a negative η suggests a larger drop on the cathode side. The value ε used in Equation (2) was obtained from photoelectron spectroscopy data.[46] The extracted trend shows that η decreases from approximately 0.3 to 0 as the transition voltage increases (Figure 4b). This indicates that lower-conductance CPTA junctions correspond to higher structural asymmetry—associated with a larger through-space—while higher-conductance junctions exhibit reduced asymmetry. This structural dependence is also reflected in the corresponding *I–V* characteristics (Supporting Information S3). These results provide a consistent interpretation of structural asymmetry in the CPTA junction, as inferred from electrical measurements.

■CONCLUSION

The performance and characteristics of single-molecule switching devices based on the structurally asymmetric CPTA molecule were systematically investigated. The CPTA molecular junction exhibited bistable conductance switching, in which conductance was reversibly modulated between LCS and HCS through the formation and closure of through-space gaps within the junction.

Quantitative analysis using the SLTT model elucidated the roles of molecular energy levels and electrode coupling strengths in determining conductance. Complementary TVS analysis provided insight into the asymmetry parameter associated with each conductance state. Together, these analyses revealed a direct correlation between structural modulation of the molecular junction and its electronic transport behavior. Notably, the results indicated that CPTA molecules anchored to the cathode electrode predominantly governed the switching mechanism.

The developed fabrication method—based on spin-coating CPTA onto nanogap electrodes—offers a simple and scalable strategy for integrating switching-capable molecules into nanoscale junctions. The intrinsic asymmetry of the CPTA molecule improves both molecular insertion efficiency and cyclic switching performance, presenting a promising route toward scalable, high-performance molecular electronic devices.

■ ASSOCIATED CONTENT

Supporting Information

Additional experimental details support the experimental result (PDF):

Figure S1. Nanogap distance tuning and conductance measurement by varying nanogap distances: electromigration and field migration in an electric field.

Figure S2. Voltage sequence for the cyclic operation of binary conductance switching.

Figure S3. Current imbalance between the positive and negative bias in the low-conductance state.

■ AUTHOR INFORMATION

Corresponding Authors

Hiroshi Suga − Chiba Institute of Technology, Tsudanuma, Narashino, Chiba 275-0016, Japan; orcid.org/ 0000-0003-4333-4898; Email: hiroshi-suga@it-chiba.ac.jp

Yasuhisa Naitoh − Core Electronics Research Institute, National Institute of Advanced Industrial Science and Technology (AIST), Tsukuba, Ibaraki 305-8565, Japan; orcid.org/0000-0003-2431-9625; Email: ys-naitou@aist.go.jp
Kazuhito Tsukagoshi − International Center for Materials Nanoarchitectonics, National Institute for Materials Science, Tsukuba 305-0044 Ibaraki, Japan; orcid.org/0000-0001-9710-2692; Email: TSUKAGOSHI.Kazuhito@nims.go.jp

Authors
Masato Takei − Chiba Institute of Technology, Narashino, Chiba 275-0016, Japan; International Center for Materials Nanoarchitectonics (WPI-MANA), National Institute for Materials Science (NIMS), Tsukuba, Ibaraki 305-0044, Japan; orcid.org/0000-0002-3522-0033
Akira Takatsuki − Chiba Institute of Technology, Narashino, Chiba 275-0016, Japan; International Center for Materials Nanoarchitectonics (WPI-MANA), National Institute for Materials Science (NIMS), Tsukuba, Ibaraki 305-0044, Japan; orcid.org/0000-0002-6422-6899
Katsunori Wakabayashi − Department of Nanotechnology for Sustainable Energy, School of Science and Technology, Kwansei Gakuin University, Sanda, Hyogo 669-1330, Japan; orcid.org/0000-0002-9147-9939
Satoshi Kaneko − Department of Materials Science and Engineering, School of Materials and Chemical Technology, Institute of Science Tokyo, Tokyo 152-8550, Japan; orcid.org/0000-0002-0351-6681

Author Contributions
M. Takei, A. Takatsuki, K. Tsukagoshi, and H, Suga fabricated and performed electrical measurements. M. Takei, H. Suga. S. Kaneko. K. Wakabayashi, Y. Naitoh, and K. Tsukagoshi analyzed the conduction properties of the CPTA single-molecule junction system. M. Takei, H. Suga, and K. Tsukagoshi conducted the experiments and prepared the manuscript.
All authors reviewed and approved the final version of the manuscript. The authors contributed equally to this work.

■ ACKNOWLEDGMENTS

The authors thank K. Homma (Institute of Science Tokyo) for the valuable discussions on single-molecule junctions. This work was supported by JSPS KAKENHI Grant Number 20K05291, Japan.

■ REFERENCES

(1) Park, H.; Park, J.; Lim, A. K. L.; Anderson, E. H.; Alivisatos, A. P.; McEuen, P. L. Nanomechanical Oscillations in a Single-C_{60} Transistor. *Nature* **2000**, *407* (6800), 57–60.

(2) Xie, X.; Li, P.; Xu, Y.; Zhou, L.; Yan, Y.; Xie, L.; Jia, C.; Guo, X. Single-Molecule Junction: A Reliable Platform for Monitoring Molecular Physical and Chemical Processes. *ACS Nano* **2022**, *16* (3), 3476–3505.

(3) Huang, T.; Zhao, J.; Feng, M.; Popov, A. A.; Yang, S.; Dunsch, L.; Petek, H. A Molecular Switch Based on Current-Driven Rotation of an Encapsulated Cluster within a Fullerene Cage. *Nano Lett.* **2011**, *11* (12), 5327–5332.

(4) Suga, H.; Suzuki, H.; Shinomura, Y.; Kashiwabara, S.; Tsukagoshi, K.; Shimizu, T.; Naitoh, Y. Highly Stable, Extremely High-Temperature, Nonvolatile Memory Based on Resistance Switching in Polycrystalline Pt Nanogaps. *Sci. Rep.* **2016**, *6* (1), 34961.

(5) Jäger, C. M.; Schmaltz, T.; Novak, M.; Khassanov, A.; Vorobiev, A.; Hennemann, M.; Krause, A.; Dietrich, H.; Zahn, D.; Hirsch, A.; Halik, M.; Clark, T. Improving the Charge Transport in Self-Assembled Monolayer Field-Effect Transistors: From Theory to Devices. *J. Am. Chem. Soc.* **2013**, *135* (12), 4893–4900.

(6) Grossi, A.; Perez, E.; Zambelli, C.; Olivo, P.; Miranda, E.; Roelofs, R.; Woodruff, J.; Raisanen, P.; Li, W.; Givens, M.; Costina, I.; Schubert, M. A.; Wenger, C. Impact of the Precursor Chemistry and Process Conditions on the Cell-to-Cell Variability in 1T-1R Based HfO_2 RRAM Devices. *Sci. Rep.* **2018**, *8* (1), 11160.

(7) Zhu, K.; Liang, X.; Yuan, B.; Villena, M. A.; Wen, C.; Wang, T.; Chen, S.; Hui, F.; Shi, Y.; Lanza, M. Graphene–Boron Nitride–Graphene Cross-Point Memristors with Three Stable Resistive States. *ACS Appl. Mater. Interfaces* **2019**, *11* (41), 37999–38005.

(8) Sun, Y.-L.; Nabatame, T.; Chung, J. W.; Sawada, T.; Miura, H.; Miyamoto, M.; Tsukagoshi, K. Compositional Changes between Metastable SnO and Stable SnO_2 in a Sputtered Film for P-Type Thin-Film Transistors. *Thin Solid Films* **2024**, *807*, 140548.

(9) Tsukagoshi, K.; Umeta, Y.; Suga, H. C_{60} Nanowire Two-State Resistance Switching: Fabrication and Electrical Characterizations. *Jpn. J. Appl. Phys.* **2022**, *61* (SD), SD0804.

(10) Umeta, Y.; Suga, H.; Takeuchi, M.; Zheng, S.; Wakahara, T.; Wang, Y.-C.; Naitoh, Y.; Lu, X.; Kumatani, A.; Tsukagoshi, K. Stable Resistance Switching in Lu N@C_{80} Nanowires Promoted by the Endohedral Effect: Implications for Single-Fullerene Motion Resistance Switching. *ACS Appl. Nano Mater.* **2021**, *4* (8), 7935–7942.

(11) Umeta, Y.; Suga, H.; Takeuchi, M.; Zheng, S.; Wakahara, T.; Naitoh, Y.; Tsukagoshi, K. C_{60} -Nanowire Two-State Resistance Switching Based on Fullerene Polymerization/Depolymerization. *ACS Appl. Nano Mater.* **2021**, *4* (1), 820–825.

(12) Takei, M.; Takeuchi, M.; Suga, H.; Wakahara, T.; Wakabayashi, K.; Okada, S.; Tsukagoshi, K. Electromechanical Switching of a C_{60} Chain in a Nanogap. *ACS Appl. Electron. Mater.* **2023**, *5* (6), 3184–3189.

(13) Takei, M.; Hirama, T.; Suga, H.; Wakabayashi, K.; Tsukagoshi, K. Effective Conduction Path of a C_{60} Chain in a Nanogap Electrode. *ACS Appl. Electron. Mater.* **2024**, *6* (3), 1740–1745. https://doi.org/10.1021/acsaelm.3c01656.

(14) Takeuchi, M.; Umeta, Y.; Suga, H.; Wakahara, T.; Wang, Y.-C.; Naitoh, Y.; Wakabayashi, K.; Tsukagoshi, K. Fullerene Nanostructure-Coated Channels Activated by Electron Beam Lithography for Resistance Switching. *ACS Appl. Nano Mater.* **2022**, *5* (5), 6430–6437.

(15) Hirama, T.; Takei, M.; Motoyama, H.; Ohta, M.; Suga, H.; Wakahara, T.; Tsukagoshi, K. Resistance Switch in a Minimal-Fullerene Chain in Vertically Stacked Electrodes. *ACS Appl. Electron. Mater.* **2024**, *6* (5), 3403–3408.

(16) Meng, L.; Xin, N.; Hu, C.; Sabea, H. A.; Zhang, M.; Jiang, H.; Ji, Y.; Jia, C.; Yan, Z.; Zhang, Q.; Gu, L.; He, X.; Selvanathan, P.; Norel, L.; Rigaut, S.; Guo, H.; Meng, S.; Guo, X. Dual-Gated Single-Molecule Field-Effect Transistors beyond Moore's Law. *Nat. Commun.* **2022**, *13* (1), 1410.

(17) Kobayashi, S.; Mori, S.; Iida, S.; Ando, H.; Takenobu, T.; Taguchi, Y.; Fujiwara, A.; Taninaka, A.; Shinohara, H.; Iwasa, Y. Conductivity and Field Effect Transistor of La_2@C_{80} Metallofullerene. *J. Am. Chem. Soc.* **2003**, *125* (27), 8116–8117.

(18) Pyo, A. G. T.; Woodside, M. T. Memory Effects in Single-Molecule Force Spectroscopy Measurements of Biomolecular Folding. *Phys. Chem. Chem. Phys.* **2019**, *21* (44), 24527–24534.

(19) Quek, S. Y.; Kamenetska, M.; Steigerwald, M. L.; Choi, H. J.; Louie, S. G.; Hybertsen, M. S.; Neaton, J. B.; Venkataraman, L. Mechanically Controlled Binary Conductance Switching of a Single-Molecule Junction. *Nat. Nanotechnol.* **2009**, *4* (4), 230–234.

(20) Du, S.; Hashikawa, Y.; Ito, H.; Hashimoto, K.; Murata, Y.; Hirayama, Y.; Hirakawa, K. Inelastic Electron Transport and Ortho–Para Fluctuation of Water Molecule in H_2O@C_{60} Single Molecule Transistors. *Nano Lett.* **2021**, *21* (24), 10346–10353.

(21) Zang, Y.; Fung, E.-D.; Fu, T.; Ray, S.; Garner, M. H.; Borges, A.; Steigerwald, M. L.; Patil, S.; Solomon, G.; Venkataraman, L. Voltage-Induced Single-Molecule Junction Planarization. *Nano Lett.* **2021**, *21* (1), 673–679.

(22) Zou, Y.-L.; Liang, Q.-M.; Lu, T.; Li, Y.-G.; Zhao, S.; Gao, J.; Yang, Z.-X.; Feng, A.; Shi, J.; Hong, W.; Tian, Z.-Q.; Yang, Y. A van Der Waals Heterojunction Strategy to Fabricate Layer-by-Layer Single-Molecule Switch. *Sci. Adv.* **2023**, *9* (6), eadf0425.

(23) Kaneko, S.; Murai, D.; Marqués-González, S.; Nakamura, H.; Komoto, Y.; Fujii, S.; Nishino, T.; Ikeda, K.; Tsukagoshi, K.; Kiguchi, M. Site-Selection in Single-Molecule Junction for Highly Reproducible Molecular Electronics. *J. Am. Chem. Soc.* **2016**, *138* (4), 1294–1300.

(24) Chandler, H. J.; Stefanou, M.; Campbell, E. E. B.; Schaub, R. Li@C_{60} as a Multi-State Molecular Switch. *Nat. Commun.* **2019**, *10* (1), 2283.

(25) Magyarkuti, A.; Balogh, Z.; Mezei, G.; Halbritter, A. Structural Memory Effects in Gold–4,4′-Bipyridine–Gold Single-Molecule Nanowires. *J. Phys. Chem. Lett.* **2021**, *12* (7), 1759–1764.

(26) Tan, Z.; Zhang, D.; Tian, H.-R.; Wu, Q.; Hou, S.; Pi, J.; Sadeghi, H.; Tang, Z.; Yang, Y.; Liu, J.; Tan, Y.-Z.; Chen, Z.-B.; Shi, J.; Xiao, Z.; Lambert, C.; Xie, S.-Y.; Hong, W. Atomically Defined Angstrom-Scale All-Carbon Junctions. *Nat. Commun.* **2019**, *10* (1), 1748.

(27) Homma, K.; Kaneko, S.; Tsukagoshi, K.; Nishino, T. Intermolecular and Electrode-Molecule Bonding in a Single Dimer Junction of Naphthalenethiol as Revealed by Surface-Enhanced Raman Scattering Combined with Transport Measurements. *J. Am. Chem. Soc.* **2023**, *145* (29), 15788–15795.

(28) Nakaya, M.; Aono, M.; Nakayama, T. Ultrahigh-Density Data Storage into Thin Films of Fullerene Molecules. *Jpn. J. Appl. Phys.* **2016**, *55* (11), 1102B4.

(29) Isshiki, Y.; Fujii, S.; Nishino, T.; Kiguchi, M. Fluctuation in Interface and Electronic Structure of Single-Molecule Junctions Investigated by Current versus Bias Voltage Characteristics. *J. Am. Chem. Soc.* **2018**, *140* (10), 3760–3767.

(30) Yan, Z.; Li, X.; Li, Y.; Jia, C.; Xin, N.; Li, P.; Meng, L.; Zhang, M.; Chen, L.; Yang, J.; Wang, R.; Guo, X. Single-Molecule Field Effect and Conductance Switching Driven by Electric Field and Proton Transfer. *Sci. Adv.* **2022**, *8* (12), eabm3541.

(31) Beebe, J. M.; Kim, B.; Frisbie, C. D.; Kushmerick, J. G. Measuring Relative Barrier Heights in Molecular Electronic Junctions with Transition Voltage Spectroscopy. *ACS Nano* **2008**, *2* (5), 827–832.

(32) Song, H.; Kim, Y.; Jeong, H.; Reed, M. A.; Lee, T. Intrinsic Charge Transport of Conjugated Organic Molecules in Electromigrated Nanogap Junctions. *J. Appl. Phys.* **2011**, *109* (10), 102419.

(33) Trouwborst, M. L.; Martin, C. A.; Smit, R. H. M.; Guédon, C. M.; Baart, T. A.; Van Der Molen, S. J.; Van Ruitenbeek, J. M. Transition Voltage Spectroscopy and the Nature of Vacuum Tunneling. *Nano Lett.* **2011**, *11* (2), 614–617.

(34) Mirjani, F.; Thijssen, J. M.; Van Der Molen, S. J. Advantages and Limitations of Transition Voltage Spectroscopy: A Theoretical Analysis. *Phys. Rev. B* **2011**, *84* (11), 115402.

(35) Artés, J. M.; López-Martínez, M.; Giraudet, A.; Díez-Pérez, I.; Sanz, F.; Gorostiza, P. Current–Voltage Characteristics and Transition Voltage Spectroscopy of Individual Redox Proteins. *J. Am. Chem. Soc.* **2012**, *134* (50), 20218–20221.

(36) Markussen, T.; Chen, J.; Thygesen, K. S. Improving Transition Voltage Spectroscopy of Molecular Junctions. *Phys. Rev. B* **2011**, *83* (15), 155407.

(37) Chen, J.; Markussen, T.; Thygesen, K. S. Quantifying Transition Voltage Spectroscopy of Molecular Junctions: *Ab Initio* Calculations. *Phys. Rev. B* **2010**, *82* (12), 121412.

(38) Park, H.; Lim, A. K. L.; Alivisatos, A. P.; Park, J.; McEuen, P. L. Fabrication of Metallic Electrodes with Nanometer Separation by Electromigration. *Appl. Phys. Lett.* **1999**, *75* (2), 301–303.

(39) Suga, H.; Sumiya, T.; Furuta, S.; Ueki, R.; Miyazawa, Y.; Nishijima, T.; Fujita, J.; Tsukagoshi, K.; Shimizu, T.; Naitoh, Y. Single-Crystalline Nanogap Electrodes: Enhancing the Nanowire-Breakdown Process with a Gaseous Environment. *ACS Appl. Mater. Interfaces* **2012**, *4* (10), 5542–5546.

(40) Suga, H.; Suzuki, H.; Otsu, K.; Abe, T.; Umeta, Y.; Tsukagoshi, K.; Sumiya, T.; Shima, H.; Akinaga, H.; Naitoh, Y. Feedback Electromigration Assisted by Alternative Voltage Operation for the Fabrication of Facet-Edge Nanogap Electrodes. *ACS Appl. Nano Mater.* **2020**, *3* (5), 4077–4083.

(41) Simmons, J. G. Generalized Formula for the Electric Tunnel Effect between Similar Electrodes Separated by a Thin Insulating Film. *J. Appl. Phys*. **1963**, *34* (6), 1793–1803.

(42) Naitoh, Y.; Tani, Y.; Koyama, E.; Nakamura, T.; Sumiya, T.; Ogawa, T.; Misawa, G.; Shima, H.; Sugawara, K.; Suga, H.; Akinaga, H. Single-Molecular Bridging in Static Metal Nanogap Electrodes Using Migrations of Metal Atoms. *J. Phys. Chem. C* **2020**, *124* (25), 14007–14015.

(43) Naitoh, Y. STM Observation of Resistance Switching of Nanogap Structure. *2016 IEEE 16th International Conference on Nanotechnology (IEEE-NANO),* IEEE, Sendai, Japan, **2016**, 792–794.

(44) Tian, Z.; Yu, D.; Ren, Z.; Tian, J.; Ren, L.; Fu, Y. Atomic-Sized Pd Tunneling Junction Memory with 25ns Switching Capacity and Enhanced Endurance. *2022 IEEE International Symposium on Circuits and Systems (ISCAS)*, IEEE, Austin, TX, USA, **2022**, 3418–3422.

(45) Tian, Z.; Yao, G.; Ren, Z.; Yu, D.; Tian, J.; Li, M.; Peng, P.; Ren, L.; Liu, F.; Fu, Y. Metal Nanogap Memory: Performances and Switching Mechanism. *ACS Appl. Mater. Interfaces* **2024**, *16* (20), 26360–26373.

(46) Yang, Z.; Zhong, M.; Liang, Y.; Yang, L.; Liu, X.; Li, Q.; Zhang, J.; Xu, D. SnO_2 -C_{60} Pyrrolidine Tris-Acid (CPTA) as the Electron Transport Layer for Highly Efficient and Stable Planar Sn-Based Perovskite Solar Cells. *Adv. Funct. Mater.* **2019**, *29* (42), 1903621.

(47) De Renzi, V.; Rousseau, R.; Marchetto, D.; Biagi, R.; Scandolo, S.; Del Pennino, U. Metal Work-Function Changes Induced by Organic Adsorbates: A Combined Experimental and Theoretical Study. *Phys. Rev. Lett.* **2005**, *95* (4), 046804.

(48) Hofmann, O. T.; Deinert, J.-C.; Xu, Y.; Rinke, P.; Stähler, J.; Wolf, M.; Scheffler, M. Large Work Function Reduction by Adsorption of a Molecule with a Negative Electron Affinity: Pyridine on ZnO(1010). *J Chem Phys*. **2013**, *139* (17), 174701.

(49) Niederreiter, M.; Cartus, J.; Werkovits, A.; Hofmann, O. T.; Risse, T.; Sterrer, M. Interplay of Adsorption Geometry and Work Function Evolution at the TCNE/Cu(111) Interface. *J. Phys. Chem. C* **2023**, *127* (50), 24266–24273.

(50) Arabnejad, S.; Pal, A.; Yamashita, K.; Manzhos, S. Effect of Nuclear Motion on Charge Transport in Fullerenes: A Combined Density Functional Tight Binding—Density Functional Theory Investigation. *Front. Energy Res.* **2019**, *7*, 3.

(51) Nahm, T.-U.; Jung, R.; Kim, J.-Y.; Park, W.-G.; Oh, S.-J.; Park, J.-H.; Allen, J. W.; Chung, S.-M.; Lee, Y. S.; Whang, C. N. Electronic Structure of Disordered Au-Pd Alloys Studied by Electron Spectroscopies. *Phys. Rev. B* **1998**, *58* (15), 9817–9825.

444 TOC

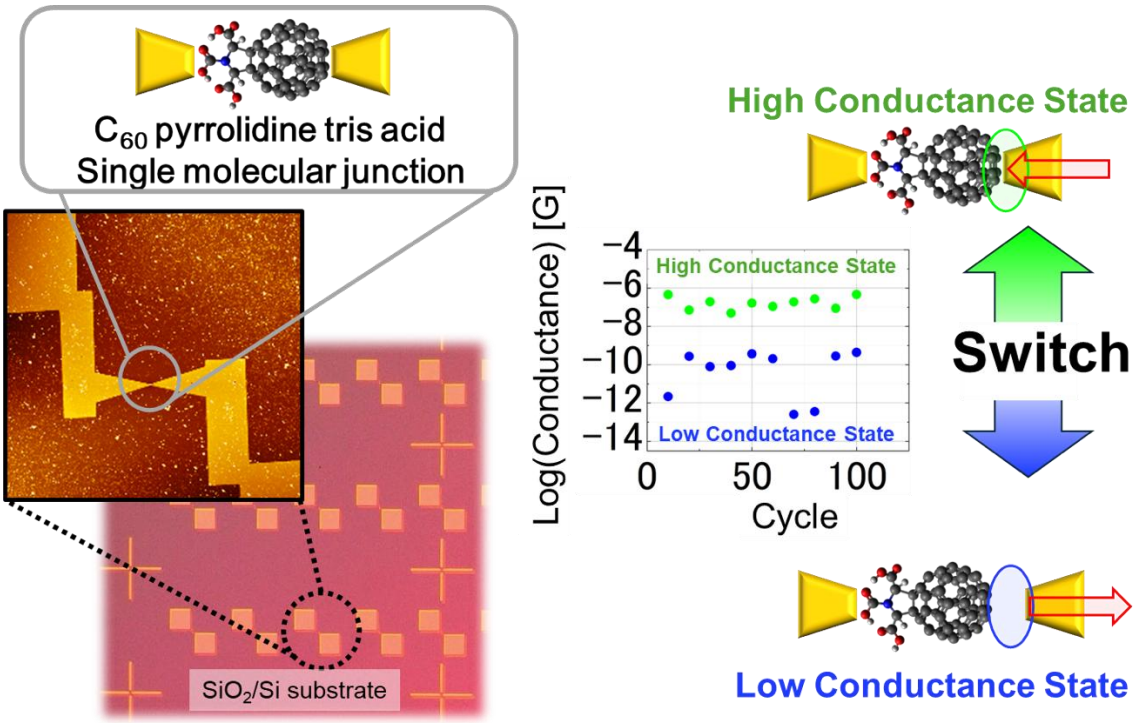

445

446